ELSEVIER

Journal of Nuclear Materials 241–243 (1997) 902–907

journal of nuclear materials

ELM structure in the boundary plasma on COMPASS-D

S.J. Fielding *, K.B. Axon, M.G. Booth, R.J. Buttery, J. Dowling, D. Gates, C. Hunt, C. Silva [1], M. Valovic

UKAEA Fusion (Euratom Fusion Association), Abingdon, Oxon OX14 3DB, UK

Abstract

ELM experimental analysis on COMPASS-D, which has previously catalogued magnetic precursor behaviour, has been extended to consider effects in the SOL. ELM precursors are observed at the divertor. Profile changes are measured with high resolution and power and particle losses in ELMs are estimated. High speed videos of an ELM show a turbulent edge extending to the outboard limiter, in broad agreement with reciprocating probe observations. A model which describes well the magnetic features of the ELM, is being extended to include predictions of power deposition structure at the divertor target, for comparison with experimental data.

Keywords: COMPASS-D; Boundary plasma; Boundary MHD; Improved confinement mode; Energy deposition

1. Introduction

ELMs are a beneficial feature of the H-mode in terms of density and impurity control, but can lead to high exhaust power transients on the divertor target. It has been generally assumed in the past that the enhanced power and particle fluxes associated with the ELM are driven by a simple increase in the edge heat and particle diffusivity, leading to toroidally uniform deposition on the target plates. However, magnetic coil array measurements, particularly on COMPASS-D which has a sensitive and comprehensive Mirnov coil system, suggest that there is a spatial structure to ELM pre-cursors and to the main ELM event itself [1,2]. The magnetic signals indicate that an ELM generally has rotating helical precursors which grow rapidly before the D_α spike, on a timescale of tens of μs. During the fast D_α rise the precursors usually combine to give the appearance of a non-sinusoidal travelling wave with toroidal velocity component of ~ 30–50 km/s. An ergodised-magnetic-field model of the plasma inside the separatrix has been developed [3] which matches magnetic perturbations at the coil locations with observations during an ELM. The model predicts a large increase in diffusivity near the plasma boundary and a perturbation to the scrape-off layer. This paper presents detailed experimental observations of the effect of ELMs on the scrape-off layer and divertor plasma in COMPASS-D, in an attempt to compare these with predictions from the model. ELM theory is still very incomplete and the motivation for the study is to provide experimental detail and modelling ideas to guide theoretical progress and to assist in the development of ELM control techniques.

2. Experimental observations

We use as a reference discharge, an Ohmic H-mode in single null divertor geometry ($R = 0.557$ m, $a_{sep} = 0.175$ m, $\kappa = 1.6$, $I_p = 180$ kA, $B_T = 1.1$ T, $q_{95} = 3.3$), which can be repeatedly reproduced provided that boronisation is still active (within ~ 100 shots of last boronisation). Fig. 1 shows how the discharge evolves with increasing density into H-mode with type III ELMs, an ELM-free period and then regular large amplitude ELMs with a typical repetition frequency of 500 Hz, where discharge conditions reach an equilibrium. Observations reported here refer to these latter large ELMs, which have some of the characteristics of type I ELMs, but it is difficult to confirm this unambiguously in Ohmic discharges where power cannot

* Corresponding author. Fax: +44-1235 464192.

[1] Permanent address: Instituto Superior Tecnico, Assoc. Euratom-IST, Lisbon, Portugal.

PII S0022-3115(96)00629-0

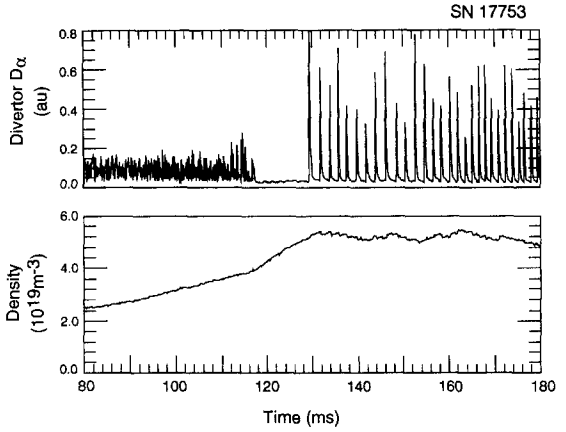

Fig. 1. Divertor D_α and line average density for a representative shot from reference discharge set; Ohmic heating, $I_p = 180$ kA, $B_T = 1.1$ T.

be varied independently. The principal ELM diagnostics, other than spatially distributed D_α views, which for divertor target observations are tightly focused onto the inner strike point, are: (a) fast reciprocating probe (60 mm stroke in 60 ms), situated at the top of plasma close to the stagnation point, fitted with multiple graphite tips and operated in triple probe mode; (b) divertor target embedded probe array with particularly high spatial resolution (5 mm) over the full 200 mm width of the target; (c) 3 poloidal arrays of Mirnov coils at different toroidal locations, separated by 45° and 180°. All data can be sampled at up to 1 MHz for a limited time window during the discharge.

2.1. ELM precursors

Magnetic precursors to ELMs on COMPASS-D have been described in detail previously [2]. Fig. 2 shows that precursor behaviour is also observed in the D_α target light emission, with increased signal being detected at a similar time to the growth of the coherent magnetic feature seen by the Mirnov coil, up to 100 μs before the start of the D_α increase at the mid-plane and the rapid rise at the target. Clear precursors are also seen on the target probe array floating potentials, in the SOL current (see below) and in probe ion currents, although this latter effect is not as well-defined. Precursors in the probe signals are, however, not seen in advance of magnetic features, as they have been on TCV [4]. Magnetic activity in the confined plasma therefore appears to result in discernable effects at the divertor target prior to the main ELM event.

2.2. SOL profiles

Plasma profile changes in the scrape-off layer have been measured by box-car techniques (repeated synchronised sampling using the ELM peak for timing registration) applied to the series of ELMs during the stroke of the reciprocating probe. Fig. 3 shows a comparison of T_e and n_e profiles 500 μs before an ELM (regarded as ELM-free discharge conditions) and at the ELM peak (poloidal flux

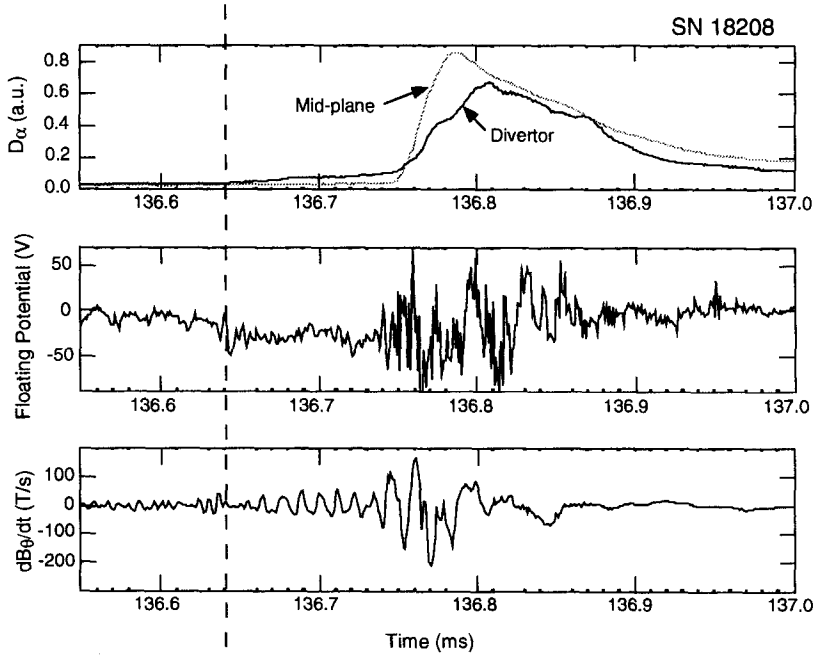

Fig. 2. ELM precursor features seen in divertor D_α, embedded probe array floating potential (outboard of outer strike-point) and outboard Mirnov coil signals.

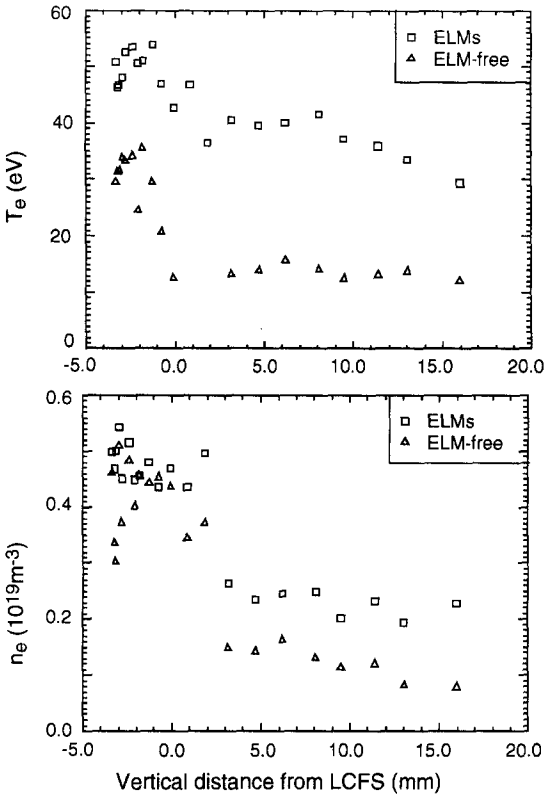

Fig. 3. Profiles of temperature and density in the SOL as measured by the reciprocating probe. Each point refers to a different ELM from box-car analysis of data taken in the reference discharge set.

compression ~ 2.5 from probe position to mid-plane). The profiles appear somewhat complex in shape, which may be an artefact of the measurement procedure (each point corresponds to a different ELM) and are difficult to reconcile with simple exponential decay. However some general observations can be made. There is a significant enhancement in both density and temperature in the SOL during an ELM (observed out to at least 60 mm from the separatrix). The measurements do not however distinguish between broadening of the profiles or raising of a plateau value. The general features of the particle behaviour are confirmed by multichannel FIR interferometry, which shows a density increase of about a factor of 2 in the outermost channel during an ELM, consistent in magnitude with the probe profile changes and a density fall on the adjacent channel 50 ms inboard, consistent with an abrupt expulsion of particles from the confined edge into the SOL.

The embedded Langmuir probe array in the divertor target gives high resolution divertor plasma T_e and n_e profiles during ELMs. These single probes are swept at 100 Hz and an average characteristic is built up over a series of ELMs again using box-car techniques. Fig. 4 shows a comparison of profiles, at the divertor target, before an ELM and at the ELM peak (poloidal flux compression ~ 4.5 from divertor target to mid-plane) with radial decay lengths (exponential fits) given in Table 1. Also shown for reference are profiles from the lower density L-mode portion of the discharge. It can be seen that the heat flux profile is broadened by approximately a factor of 2 during the ELM, with up to a 6-fold increase in power density. Comparison between these profiles and those from the reciprocating probe show: (1) no significant temperature gradient along the field lines, $T_e^{probe} \sim T_e^{target}$, both between and during ELMs. (2) Approximate pressure balance in ELM-free conditions (between ELMs): from the data $p^{probe} \sim p^{target}$, as opposed to the expected ratio $p^{probe}/p^{target} = 2$ for a collisionless sheath at the divertor target. However, no correction has been applied for sheath effects at the reciprocating probe (these could increase the inferred density by up to a factor of 2) and errors resulting from flux surface mapping uncertainties are substantial. (3) Probable pressure imbalance at the ELM peak with ob-

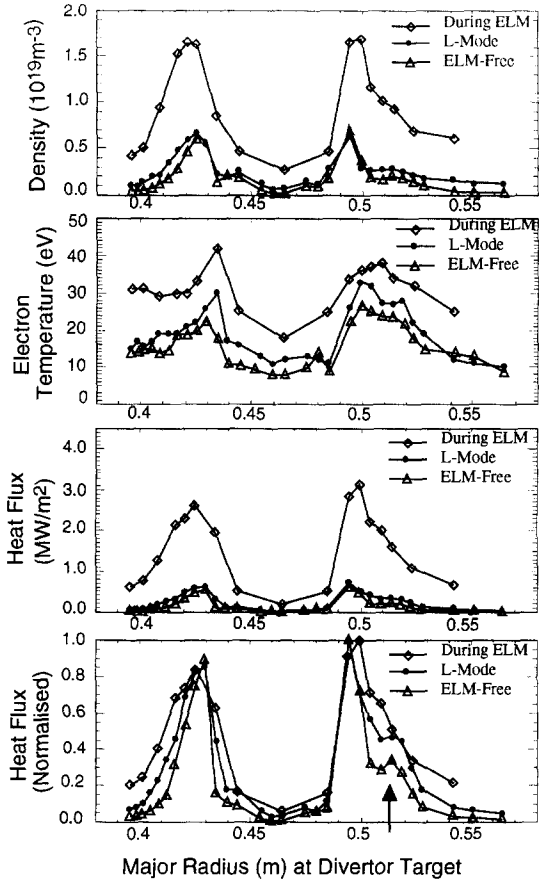

Fig. 4. Profiles of density temperature and heat flux ($8j_{sat}(kT_e/e)$) from the embedded probe array, from box-car averaging of shots in the reference set. Profiles are mapped in major radius at the divertor target. Arrow indicates distorting feature, attributed to divertor currents.

Table 1
Divertor target plasma decay lengths

	Divertor target	
	inner λ (mm)	outer λ (mm)
Density		
L-mode	14	50
ELM	20	47
ELM-free	10	22
Temperature		
L-mode	60	53
ELM	100	100
ELM-free	50	60
Heat flux [a]		
L-mode	11	26
ELM	17	32
ELM-free	8	16

[a] Heat flux computed as $8 j_{sat}(kT_e/e)$.

served $p^{probe}/p^{target} \sim 1/3$. Since the time scale to establish pressure balance at a transient event is $L/c_s \sim 250$ μs, appreciably longer than the time to the ELM peak, ~ 50 μs, then deviation from pressure equilibrium may not be unexpected.

2.3. Divertor currents

The outboard divertor profiles show a distinct distorting feature some distance away from the strike-point (arrowed in Fig. 4). This is thought to be due to the presence of additional currents, independent of the saturated ion flux, which can be more clearly shown by operating the probes with zero bias. This divertor current, which integrates across the target to approximately zero, appears to flow from the outboard (electron) side to the inboard (ion) side (i.e. in the same direction as I_p) and is in part due to thermoelectric current driven by the difference in potential between the inner and outer target sheaths. However, close to the strike points the current is reversed and appears to be due to a different mechanism since ELM precursor behaviour in the SOL currents is most marked close to the strike-points, whereas precursor effects in the floating potential, which would be expected to cause changes to thermo-electric currents, are greatest away from the strike-point region, suggesting two different effects. One possibility is the presence of SOL Pfirsch–Schluter currents, recently identified on JET [5], which are observed to flow in a narrow zone in or near to the private flux region. On COMPASS-D the peak divertor current, assuming flow parallel to the field (as has been confirmed on JFT-2 M [6]) and that it is toroidally symmetric, is ~ 200 A, about 0.1% of the plasma current, in rough agreement with tile halo current detector measurements.

2.4. Plasma loss

The particle loss in an ELM has been estimated by summing the increased particle flux measured by each target probe and assuming toroidal symmetry. Account has to be taken of particle flux amplification by recycling. The flux amplification factor F (ratio of particle flux to the divertor to that crossing the separatrix) can be evaluated from the density behaviour [7] in L-mode ($F = 2.8$) and ELM-free H-mode ($F = 3.1$) periods in the discharge. Note that $F > 1$, denoting the global behaviour of the SOL, is not inconsistent with pressure balance along individual flux tubes. Assuming that $F \sim 3$ is retained during the ELM, the average particle loss per ELM is ~ 3% of the total particle content.

The average power loss/ELM has been estimated by toroidal integration of the divertor heat flux profile, as measured by the probe array. The power loss has also been estimated from diamagnetic loop measurements [8] and Fig. 5 shows that the agreement between the two results is surprisingly good, indicating that SOL radiation losses are not substantial (although measurement uncertainties are probably ~ 30% for each technique). Typically 4% of the plasma energy is lost in these large ELMs, which is characteristic of the fractional loss in type I ELMs reported on other devices [9]. Fig. 5 shows that high transient power to the divertor is produced by the ELM, with peak power densities ~ 3 MW/m^2 in Ohmic discharges.

2.5. Structure

High speed videos [10] of plasma visible light during an ELM (24.7 μs framing time), reveal further features.

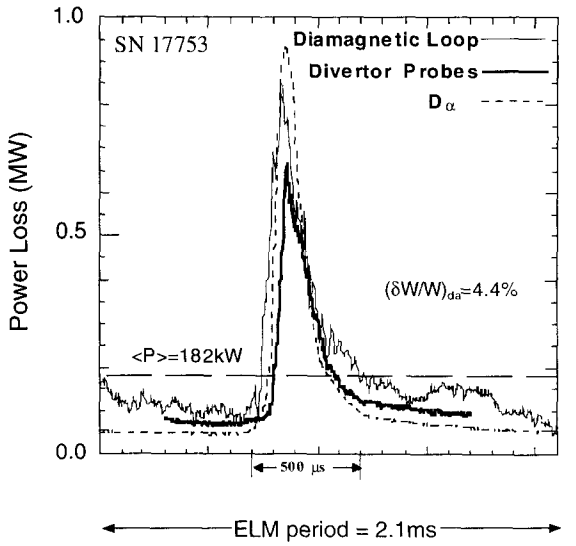

Fig. 5. Power loss during an ELM measured by fast diamagnetic loop and estimated from integrated heat flux to the divertor probes.

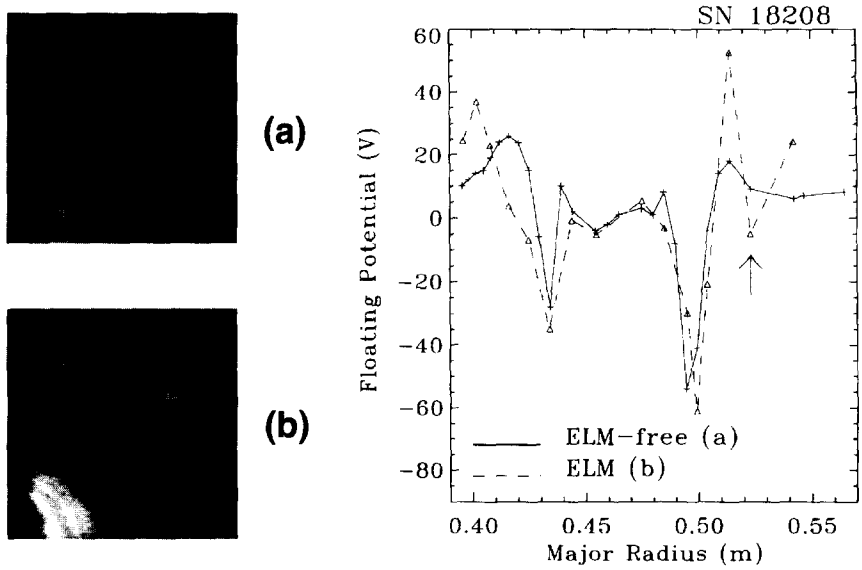

Fig. 6. High speed video pictures (24.7 μs framing time, tangential view, major radius increasing to right) before (a) and during an ELM (b) (at time of D_α peak). Multiple strike-points and a turbulent outer edge develop during the D_α rise. A second outer strike-point is indicated by the additional floating potential negative peak (arrowed).

Fig. 6 shows that at the time of the rise of the D_α there is a turbulent broadening of the outboard plasma edge, leading to enhanced interaction with the vessel surfaces, particularly near the mid-plane, with little evidence for increased interaction with the inner wall limiter. Another obvious feature is the appearance of additional outboard strike-points. Evidence of a second outboard strike-point is also seen on the target probes (see Fig. 6), which develops during the time of the D_α rise (negative peaks in the floating potential correspond to strike points). Similar features have been observed during ELMs on D-IIID [11] and JT-60 U [12]. This suggests that the ELM has coherent structure associated with it in the boundary layer. The divertor target D_α invariably shows significant frequency modulation at $\sim$ 50 kHz during the main ELM (see Fig. 2 also), which occasionally can be detected in the D_α precursor. However, analysis of the fluctuations in both j_{sat} and floating potential, using the Fourier techniques applied to the Mirnov coils, at both 50 kHz and at the higher frequencies ($\sim$ 140 kHz) seen in the magnetic signals, has not as yet revealed evidence of the rotating helical structure which is seen in the magnetic fluctuations. It should, however, be pointed out that the probe electronic analysis system had not been optimised for these fluctuation measurements.

3. Modelling

The external magnetic field perturbations during an ELM have been modelled in terms of helical filament currents parallel to the field on the relevant internal flux surfaces [3], the current varying sinusoidally with filament number to match the mode number, n. The total current in the resulting magnetic island is adjusted to give the observed amplitude of the Mirnov signals and the radial location of the filaments chosen to reproduce the observed poloidal variation at the different toroidal locations. Use of this technique for ELMs with measured $n = 4$, 5 modes predict their radial location ($q = 2.25$, 2.8, $m = 9$, 14, respectively) as $\sim$ 8–16 mm inboard of the separatrix (outboard mid-plane). At maximum mode amplitude the magnetic field braiding/ergodisation gives rise to very high values of electron thermal diffusivity ($\sim$ 10 m^2 s^{-1}). Complete loss of the outer 20 mm of plasma, based on reasonable edge ion temperature and density values, corresponds to an energy loss/ELM of $\sim$ 3%, in line with the experimental estimates of the previous section for similar ELMs. This model therefore reproduces the observed magnetic features and predicts the observed energy loss.

The modelling has now been extended to investigate the effect of the magnetic perturbations on the trajectories of field lines in the scrape-off layer. Earlier work based on externally applied perturbations [13], showed that a splitting of the strike points could be produced in the modelling (and was experimentally observed) by application of a sufficiently large perturbation (in this case $n = 1$, $m = 2$). Preliminary results from ELM modelling suggest that rotating coherent structures may be produced in the power profile on the target, although clear strike-point splitting is not yet indicated. This work is still under development.

4. Summary and conclusions

ELM experimental analysis on COMPASS-D, which has catalogued the detailed magnetic pre-cursor behaviour, has been extended to consider effects on the scrape-off-layer plasma. Pre-cursors to the main ELM event, in addition to the usual magnetic signatures, are seen in the divertor target D_α, divertor plasma floating potential and divertor currents. The observed poloidal divertor current is not fully explained by thermo-electric effects and an additional mechanism, possibly SOL Pfirsch–Schluter currents, is involved. High resolution probe array measurements in the divertor show that the heat flux profile broadens by a factor of 2 during an ELM. About 3% of the plasma particle content is transferred across the separatrix to the scrape-off layer and about 4% of the plasma energy content, leading to high power transients ~ 3 MW/m^2 for Ohmic plasmas, a factor of 6 increase on ELM-free values. High speed video pictures during an ELM support reciprocating probe profile measurements of enhanced density and temperature over a wide extent in the SOL, > 25 mm ($\sim a_s/7$) mapped to the midplane and show a turbulent broadened edge, predominantly observable on the outboard side. This latter feature, indicative of pressure driven fluctuations, plus the significant magnitude of the energy loss/ELM, suggests that these ELMs could be type I. High-speed videos also show multiple (i.e. > 2) strike-points, particularly during the early part of the main ELM event, also detected by the divertor probes. However coherent rotating structures as seen in the Mirnov coil analysis have not as yet been detected at the divertor by the probes, although oscillatory structure is seen in the D_α light emission. Modelling of the ELM magnetic signature suggests a growing edge magnetic perturbation, leading to ergodisation of the edge and plasma energy loss in good agreement with observations. The model makes specific predictions for effects in the SOL and at the divertor target which are being compared with detailed edge measurements, with a view to identifying possible power asymmetries during the ELM.

Acknowledgements

The authors are grateful for advice from Dr. A.W. Morris and Dr. D.C. Robinson and assistance from members of the COMPASS-D Team. This work is jointly funded by the UK Department of Trade and Industry and Euratom.

References

[1] M. Valovic et al., Proc. 21st EPS Conf. Montpellier (1994) Vol. I, p. 318.
[2] A. Colton et al., ELM studies on the COMPASS-D tokamak, 5th H-mode Workshop, Princeton, Plasma Phys. Controlled Fusion (1995), to be published.
[3] R.J. Buttery et al., Proc. 22nd EPS Conf. Bournemouth (1995) Vol. III, p. 273.
[4] H. Weisen et al., Ohmic H-modes in the TCV tokamak , 5th H-mode Workshop, Princeton, Plasma Phys Controlled Fusion (1995), to be published.
[5] M.J. Schaffer et al., JET - P(96) 11, Nucl. Fusion, submitted.
[6] K. Nagashima et al., J. Nucl. Mater. 220–220 (1995) 208.
[7] J.K. Ehrenberg, JET-P(95)18, Phys. Processes Interaction Fusion Plasmas Solids, to be published.
[8] M. Valovic et al., 23rd EPS Conf. Kiev, June (1996), to be presented.
[9] H. Zohm et al., Proc. 20th EPS Conf. Lisbon (1993) Vol. I, p. 19.
[10] Kodak EktaPro Model 4540, Eastman Kodak Company, San Diego, CA 92121-1097.
[11] D.N. Hill, these Proceedings, p. 182.
[12] K. Itami et al., J. Nucl. Mater. 220–220 (1995) 203.
[13] R.J. Buttery et al., Proc. 22nd EPS Conf. Bournemouth (1995) Vol. IV, p. 213.